ORIGINAL PAPER

Impact Energy Absorption Behavior of Cemented Coal Gangue-Fly Ash Backfill

Di Wu · Yu-cheng Liu · Zhi-xue Zheng · Song Wang

Abstract A drop hammer test device is employed to conduct impulse tests on the cemented coal gangue-fly ash backfill (CGFB) samples which have different solid concentrations, dimensions and curing ages. The impacting time of the drop hammer on the CGFB and the maximum rebound height of the hammer are investigated. The acoustic energy loss induced by the impact of the drop hammer on the CGFB and the impact energy absorption power of the CGFB are obtained. The results indicate that, the impact energy absorption power of the CGFB increases with the increases of its solid concentration and dimension. The impact energy also exerts influence on the energy absorption power of the CGFB. When the impact energy is lower than a critical value, the energy absorption power of the CGFB increases with the increase in the impact energy. But when the impact energy exceeds the critical value, the energy absorption power of the CGFB decreases with the increase of the impact energy. The obtained results can provide theoretical and practical guidance for preventing rock burst.

D. Wu (✉) · Y. Liu · Z. Zheng · S. Wang
Faculty of Resources and Safety Engineering, China University of Mining and Technology (Beijing), Beijing 100083, China
e-mail: tauo123@163.com

D. Wu
State Key Laboratory of Coal Resources and Safe Mining, China University of Mining and Technology, Beijing 100083, China

1 Introduction

The coal mining industry generates substantial financial revenues worldwide and these revenues are essential for the improvement of people's living standards. To date, the development of the coal mining industry has involved in people's livelihood. However, with the increase of mining depth, coal mining is associated with numerous challenges such as the prevention and treatment of high temperature and rock burst, as well as the management of large volumes of solid wastes (e.g., coal gangues).

For coal mines, rock burst refers to the dynamic process of sudden and intense release of elastic energy accumulated in coal-rock mass during mining (Dou et al. 2006; Dou and He 2001), and it is one of the most catastrophic dynamic hazards in coal mines. The destructiveness of rock burst is exacerbated with the increase of mining depth. Once rock burst occurs, the safety of miners' lives may be threatened. Moreover, rock burst may also damage underground working faces and roadways. This seriously hinders the efficient extraction of coal resources and thus results in severe economic problems. In China, coal is the primary energy resource, and almost 95 % of total coal production is from underground coal mines (Liu and

Liu 2010). Rock burst has become an indispensable issue exerting a negative impact on the underground coal mining industry. For instance:

- The rock burst of Sunjiawan Coal Mine in Fuxin, Liaoning Province, China occurred on February 14, 2005 led to 214 deaths of people.
- The rock burst in Qianqiu Coal Mine in Yima, Henan Province on November 3, 2011 killed 10 people and trapped 75 people underground.

Therefore, it is significant to forecast, prevent and manage rock burst incidents in coal mines. As an alternative solution, filling the mined-out openings can effectively relieve the damage induced by rock bursts (Cai et al. 2001; Jiang et al. 2014). This is due to the fact that the backfilled body can reduce the space for the dissipation of the energy released by rock bursts. In addition, the backfilled body can also absorb the burst energy. As to coal mines, coal gangues are the main solid wastes produced during mining. The traditional treatment of the coal gangues is to dump them in cone-shaped heaps on the ground, which results in serious social and environmental problems. For instance, the spontaneous combustion of the coal gangue piles may cause personal injuries or even deaths, and the poison released from the coal gangue heaps may contaminate underground water. However, taking advantage of the coal gangues to make backfill materials and fill the underground voids with them can not only dispose the solid wastes, but also alleviate the rock bursts. Several studies (e.g., Bian et al. 2009; Karfakis et al. 1996; Zhang and Wang 2007) have reported the utilization of coal gangues for making backfill materials. Fly ash, which is a kind of by-products generated from coal combustion, can also be applied to make the backfill materials, associated with favorable environmental and economic benefits (Horiuchi et al. 2000).

In the present study, the coal gangue and fly ash are mixed with cement and water to prepare the backfill mixture, which is called cemented coal gangue-fly ash backfill (CGFB). By admixing water and cement, the freshly prepared CGFB mixtures can be transportable through pipelines to the underground openings, and after a period of time, the backfilled CGFBs can solidify by themselves and have mechanical strength. Some studies have been conducted on the energy dissipation responses of the cemented backfills (CBs) to external force loading. Deng et al. (2010) have investigated the internal energy change and

dissipation process of CB structures under compressive stress loading. Liu et al. (2010) have carried out a study on three-dimensional energy consumption characteristics of the CBs. In addition, some other researchers (e.g., Cui and Sun 2010; Chugh et al. 2003; Fall and Samb 2009; Zheng et al. 2006) have focused their studies on the mechanical performance of the backfilled structures. However, the results obtained from the aforementioned studies are based on the fact that the backfills are under static loads. To date, few studies have been conducted on the energy variation and mechanical performance of the CBs or CGFBs under dynamic impacts.

The backfilled materials can effectively relieve the hazards caused by rock bursts by absorbing the released energy. Therefore, understanding the energy absorption properties of the backfills is helpful to the prevention of rock bursts. This has urged the authors to conduct the current study. This study has been carried out to investigate the dynamic impact energy absorption behavior of the CGFB samples (with different dimensions, mix proportions, and curing periods), and a drop-hammer test system is equipped to provide the dynamic impact. Similar studies of carrying out the drop-hammer experiment on rocks have been reported. For instance, Lin and Chen (2005) have employed a drop-hammer test to reveal the damage law of rocks. Nevertheless, when they calculate the energy absorbed by the rocks, they approximately regard the gravitational potential energy as the absorption energy, without considering other energy losses (such as the acoustic energy loss) in the dynamic impact process. Hence, a certain error is inevitable in the calculation. For this reason, this study fully considers the acoustic energy loss during the collision between the drop hammer and the backfill specimens (namely, the CGFB samples).

This paper is organized as follows: the experimental materials and methods are first presented, and after that, testing results and corresponding discussions on these outcomes are presented. Finally, the conclusions are presented.

2 Materials and Methods

2.1 Materials

The CGFB samples tested are prepared by mixing coal gangue (from a coal mine in Northwest of China), fly

ash (from a power plant near the coal mine), cement (ordinary Portland cement 425#) and water (tap water). Table 1 presents the chemical characteristics of the coal gangue and fly ash used, and Table 2 lists the grain size of the coal gangue and fly ash. Furthermore, Fig. 1 shows the particle size distributions of the coal gangue and fly ash used. The mix proportions for these four kinds of materials are presented in Table 3, and the mix proportions used are consistent with that the coal mine applies in practice. These materials are mixed and homogenized in a mixer until obtaining a homogeneous paste. The mixing time is 3 min for all mixes. After that, the plastic CGFB pastes are poured into cylindrical molds, with two types of dimensions (one is 76 mm in inner diameter and 80 mm in height, and the other is 76 mm in inner diameter and 160 mm in height). The CGFB samples are then sealed in plastic bags and cured in a

Table 1 Chemical characteristics of the coal gangue and fly ash used

	Chemical compositions (wt%)						
	SiO_2	Al_2O_3	Fe_2O_3	CaO	K_2O	TiO_2	S
Coal gangue	41.86	23.43	5.09	23.74	0.82	1.36	3.70
Fly ash	56.89	31.89	5.38	1.84	1.39	1.95	0.66

Table 2 Grain size compositions of the coal gangue and fly ash

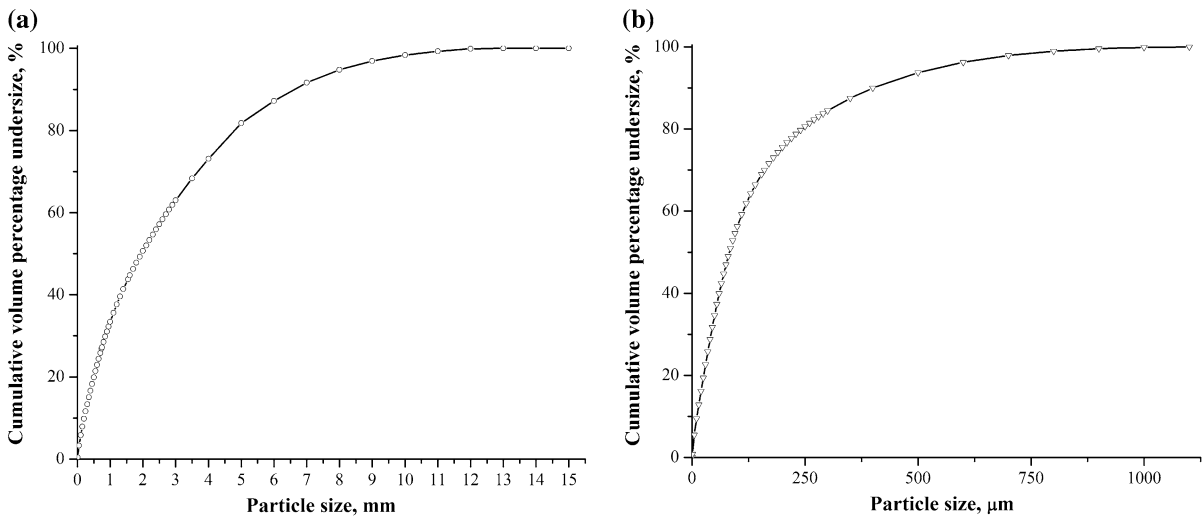|	D_{10} (µm)	D_{30} (µm)	D_{50} (µm)	D_{60} (µm)	D_{90} (µm)
Coal gangue	204.722	856.589	1952.857	2736.752	6634.312
Fly ash	10.779	43.826	82.471	112.358	400.008

Fig. 1 Particle size distributions of the coal gangue (**a**) and fly ash (**b**) used

Table 3 Mix proportions of the CGFB samples

Solids content (wt%)	Coal gangue (wt%)	Fly ash (wt%)	Cement (wt%)	Water (wt%)
78	48	20	10	20
79	49	20	10	20
80	50	20	10	20

curing chamber at the temperature of 20 ± 1 °C and for periods of 3, 7, 14, 28 and 56 days.

2.2 Test Equipment

The test device used is schematically displayed in Fig. 2. As shown in Fig. 2, the actual dynamic impact load is imitated by the impact of a steel drop hammer (1 in Fig. 2). The drop hammer in the test is cylindrical, with 80 mm in diameter and 2 kg in mass. The drop height of the hammer can be adjusted by an electric drive pusher (2 in Fig. 2), for providing different impact loads. A cross laser locator (3 in Fig. 2) is equipped to make the center point of the hammer undersurface and the center point of the top surface of the tested CGFB (10 in Fig. 2) along a plumb line, ensuring that the hammer strikes the CGFB exactly in alignment. An electromagnet (4 in Fig. 2) is fixed to attract the hammer, and an integrated control system (8 in Fig. 2) is equipped to commend the on and off of the electromagnet. When the electromagnet is turned off, the drop hammer starts to fall down. When the falling hammer passes through a correlation photoelectric door (5 in Fig. 2), a directional microphone (6 in Fig. 2) and a high-speed camera (7 in Fig. 2) are triggered to record data. The directional microphone is used to collect sound waves generated during the impact between the drop hammer and the tested CGFB. The collected acoustic wave data are recorded in an upper computer (9 in Fig. 2) in the form of acoustic waveforms. Through data processing of the acoustic waveforms, the acting time of the collision (namely, the period from

which the hammer begins to strike the CGFB column till it starts to rebound) can be figured out. The high-speed camera is employed to film the impact and bounce process of the drop hammer, and the information received in video is then recorded and processed by the upper computer. The horizontal distance between the high-speed camera and the CGFB is 0.4 m (as shown in Fig. 2), and the pixels corresponding to this distance is 240 pixel points. Therefore, the distance for a single pixel is 1.667×10^{-3} m (i.e., 0.4/240 m). According to this information, the maximum rebound height of the hammer can be figured out.

2.3 Principles of Testing

The velocity for the drop hammer when it begins to strike the CGFB can be calculated on the basis of the free-fall motion formula:

$$v_i = \sqrt{2gh_1} \tag{1}$$

where, v_i is the striking velocity of the drop hammer; g is the gravitational acceleration; and h_1 is the height of the falling hammer, which depends on the distance between the center of the drop hammer and the center of the upper surface of the CGFB.

According to the energy conservation, the following equation can be obtained:

$$E_k = \frac{1}{2}mv_i^2 \tag{2}$$

where, E_k is the impact kinetic energy of the drop hammer, and m is the mass of the hammer.

Fig. 2 The test equipment. a Physical map. b Schematic plot. 1 Drop hammer, 2 Electric drive pusher, 3 Cross laser locator, 4 Electromagnet, 5 Correlation photoelectric door, 6 Directional microphone, 7 High-speed camera, 8 Integrated control system, 9 Upper computer 10- CGFB
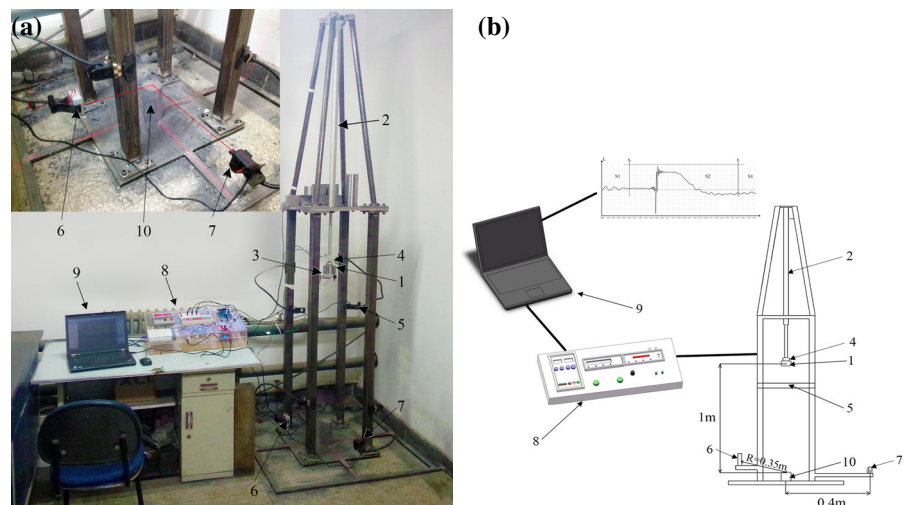
Without considering the energy loss caused by air frictional resistance (this amount of energy is so small that it can be neglected) during the falling of the drop hammer, and taking account of the acoustic energy loss induced by the collision between the hammer and the CGFB, the following expression can be obtained:

$$E_a = E_k - \frac{1}{2}mv_r^2 - E_s \qquad (3)$$

where, E_a is the energy absorbed by the CGFB, v_r is the maximum instantaneous speed when the hammer begins to rebound, and E_s is the acoustic energy.

The term v_r in Eq. (3) can be calculated by the following equation:
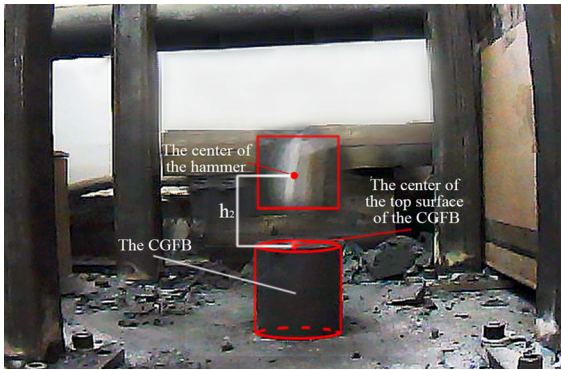
$$v_r = \sqrt{2gh_2} \qquad (4)$$

Fig. 3 Schematic diagram showing the maximum rebound height of the drop hammer

where h_2 (as shown in Fig. 3) represents the maximum rebound height of the hammer.

As illustrated in Fig. 3, the high-speed camera can record the image of the drop hammer when it rebounds at the highest height.

For simplicity, it is regarded the sound waves generated by the collision are from a point where the direct impact occurs between the falling hammer and the CGFB, and these acoustic waves are treated as spherical waves. Regarding the center of the sound receiver (i.e., directional microphone) as one point on the spherical surface, thereby the acoustic energy can be described as follows (Du et al. 2001):

$$E_s = 4\pi R^2 It \qquad (5)$$

where, I is the sound intensity, R is the distance between the center of the acoustic wave receiver and the center of the top surface of the CGFB (as shown in Fig. 2, R is 0.35 m), and t is the period of time when the sound waves get across the receiver.

An instanced sound wave recorded by the upper computer is displayed in Fig. 4. The value along the vertical axis in this figure represents the sound intensity level which can be calculated by the following formula (Cai et al. 2013):

$$L = 10 \cdot \lg \frac{I}{I_0} \qquad (6)$$

where, L is the sound intensity level, and I_0 is reference sound intensity which is generally 10^{-12} W/m^2.
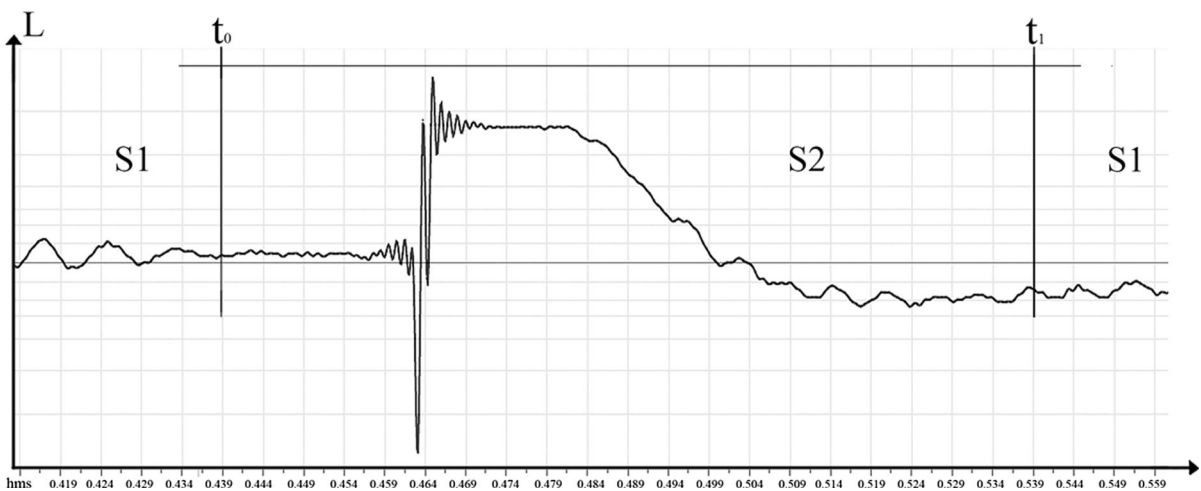

Fig. 4 An instanced acoustic waveform recorded

According to Eq. (6), the sound intensity can be figured out by the following equation:

$$I = 10^{\frac{L}{10}} \cdot I_0 \tag{7}$$

As shown in Fig. 4, if the acoustic waveform is divided into two parts (S1 and S2), of which part S1 is the floor noise section and part S2 is the segment when the impact is happening. The period for the impact (Δt) can be calculated by the following formula:

$$\Delta t = t_1 - t_0 \tag{8}$$

where, t_0 is the moment dividing part S1 and part S2 while t_1 is the one dividing part S2 and part S1.

According to Eqs (5–8) and Fig. 3, the following expression can be obtained:

$$E_s = \int_{t_0}^{t_1} 4\pi R^2 I(t) \cdot dt = 4\pi R^2 I_0 \cdot \int_{t_0}^{t_1} 10^{\frac{L(t)}{10}} \cdot dt \tag{9}$$

The term E_s (acoustic energy) in Eq. (9) can be figured out by Fourier transformation.

Integrating all of the above equations, the following expression can be obtained:

Table 4 Testing results of the impact experiments

Solids content (wt%)	Curing time (dAY)	The CGFB column height (mm)	Acoustic energy (J)	Acting time of the impact (s)	Energy absorption power (W)
78	3	80	0.0248	0.161	119.1758
		160	0.0122	0.158	121.3943
	7	80	0.0115	0.149	128.5564
		160	0.0142	0.146	131.0233
	14	80	0.0140	0.144	132.2556
		160	0.0086	0.141	134.8064
	28	80	0.0133	0.137	138.7080
		160	0.0202	0.135	140.4467
	56	80	0.0079	0.130	146.0685
		160	0.0038	0.128	148.0250
79	3	80	0.0117	0.152	125.9533
		160	0.0110	0.148	129.4500
	7	80	0.0142	0.146	130.5986
		160	0.0107	0.142	134.4169
	14	80	0.0107	0.139	137.0129
		160	0.0129	0.137	138.9489
	28	80	0.0165	0.135	140.4978
		160	0.0129	0.133	142.6624
	56	80	0.0130	0.129	146.9078
		160	0.0158	0.127	149.3024
80	3	80	0.0109	0.141	135.6000
		160	0.0136	0.14	136.4093
	7	80	0.0131	0.135	141.0304
		160	0.0129	0.133	142.9812
	14	80	0.0160	0.131	144.8664
		160	0.0198	0.129	146.9558
	28	80	0.0192	0.125	151.5592
		160	0.0191	0.124	152.5726
	56	80	0.0191	0.124	152.6774
		160	0.0189	0.123	153.7870

$$P_a = \frac{mgh_1 - mgh_2 - 4\pi R^2 I_0 \cdot \int\limits_{t_0}^{t_1} 10^{\frac{L(t)}{10}} \cdot dt}{t_1 - t_0} \qquad (10)$$

where, P_a is the energy absorbed by the CGFB per unit time, or namely, the power of the energy absorption (unit: W).

3 Results and Discussions

3.1 Testing Results

The drop hammer test device shown in Fig. 2 is used to conduct the impact experiment on the CGFB samples with different solid concentrations (78, 79 and 80 wt%) and heights (80 and 160 mm but with the same diameter of 76 mm) cured for varied periods (3, 7, 14, 28 and 56 day). In the test, the height between the center of the drop hammer and the center of the upper surface of the CGFB sample is always kept at 1 m. There are a total number of 30 kinds of CGFB samples (3 kinds of mix proportions in 2 kinds of dimensions and cured for 5 kinds of ages). Each kind of CGFB samples are prepared and tested in triplicate, and the average testing data are taken. The corresponding experimental results are tabulated in Table 4.

3.2 Discussions

3.2.1 Effect of Solids Content on the Impact Energy Absorption Power of the CGFB

According to the data presented in Table 4, the effect of the CGFB's solids content on the impact energy absorption power of the CGFB versus curing time can be obtained and the outcomes are illustrated in Fig. 5a, b. The energy absorption power of the CGFB increases with the increase of its solid concentration, regardless of the height of the CGFB sample is 80 or 160 mm. This is because with the increase of solids content, more solid matter can participate in the absorption of impact energy per unit time. In addition, from Fig. 5 it can also be observed that, the energy absorption power increment in the CGFB with the solid concentration increasing from 79–80 wt% is significantly greater than that from 78–79 wt%. Taking the CGFB sample which is 80 mm in height and cured for 28 days for instance, as its solid concentration increases from 78–79 wt%, its energy absorption power increment is 1.8 W. While the increase in the energy absorption power of the CGFB is 11.1 W when its solid concentration rises from 79–80 wt%. This demonstrates that, the higher the solid concentration of the CGFB is, the greater its impact energy absorption power is the results discussed above indicate that,
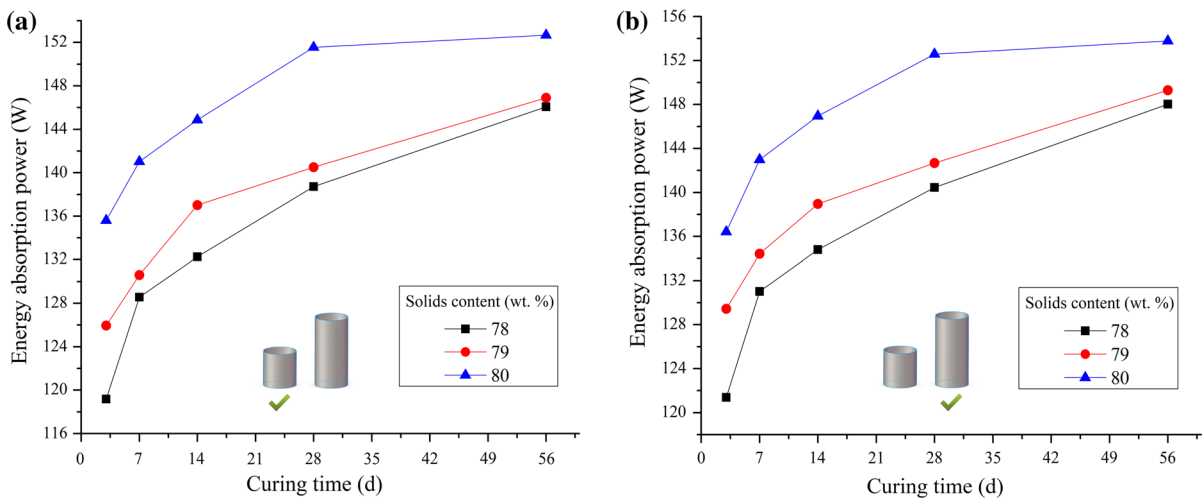

Fig. 5 Effect of solids content on the energy absorption power of the CGFB. **a** The CGFB specimen height is 80 mm. **b** The CGFB specimen height is 160 mm

increasing the solid concentration of the CGFB is in favor of absorbing more impact energy in unit time. Therefore in practice, it is better to fill the mined-out openings with more solid materials, which can help to absorb more energy released by rock bursts.

3.2.2 Effect of Dimension of the CGFB on its Impact Energy Absorption Power

Based on the corresponding experimental data listed in Table 4, the influence of the dimension of the CGFB sample on its impact energy absorption power with the elapse of curing time can be obtained, and the results are demonstrated in Fig. 6a–c. As shown in these three figures, the energy absorption power of the CGFB

increases with increasing its height, regardless of the solid concentration of the CGFB is 78, 79, or 80 wt %. This is due to the fact that, as the dimension of the CGFB increases, the volume of the CGFB also increases, which is beneficial for the CGFB structure to absorb more impact energy. The relevant practical implication is that, the fuller the underground voids are filled, the smaller the rock burst induced damage is.

3.2.3 Effect of Impact Energy on the Impact Energy Absorption Power of the CGFB

The drop impact energy can be varied by changing the falling height of the drop hammer as well as its mass. The energy absorption power of the CGFB samples
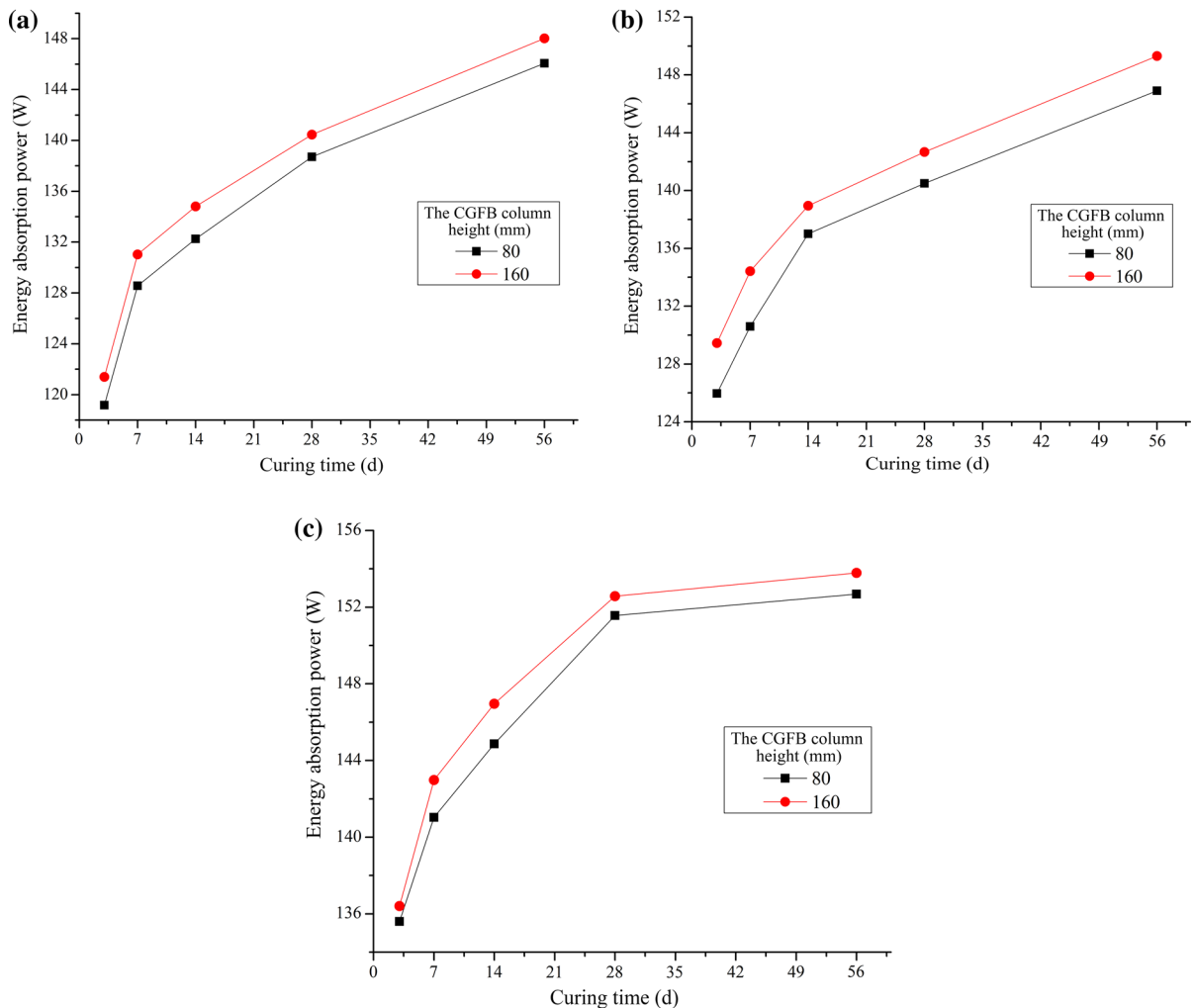

Fig. 6 Effect of dimension on the energy absorption power of the CGFB. **a** The CGFB solids content is 78 wt%. **b** The CGFB solids content is 79 wt%. **c** The CGFB solids content is 80 wt%
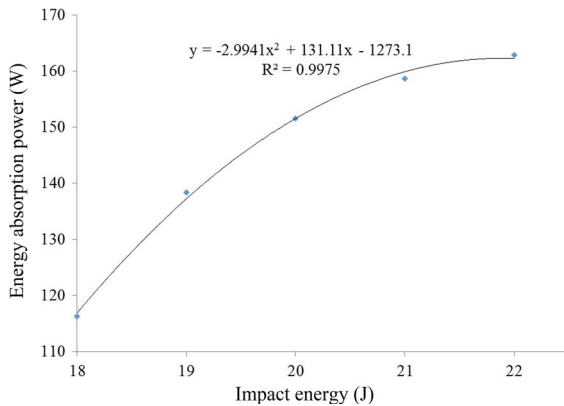
Fig. 7 Evolution of the energy absorption power of the CGFB versus impact energy

under different impact energy is demonstrated in this section. Taking the CGFB sample which is 80 wt% in solid concentration and 80 mm in height and cured for 28 day as an example, the evolution of its energy absorption power versus the impact energy is presented in Fig. 7. It can be discovered form Fig. 7 that, the energy absorption power of the CGFB increases with the increase in the impact energy, and the relation between them can be approximately represented by a quadratic function as follows (with the correlation coefficient (R) of 0.9987):

$$y = -2.9941x^2 + 131.11x - 1273.1 \quad (11)$$

where, y is the energy absorption power of the CGFB, and x is the impact energy.

A possible prediction can be made that, there exists a certain critical value for the impact energy, corresponding to the maximum energy absorption power of the CGFB. Hereafter, if the impact energy continues to increase, the energy absorption power for the CGFB will gradually decrease.

4 Conclusions

1. From the perspective of energy transfer, the moderating effect of backfilled materials (e.g., CGFB in the present study) on rock bursts is discussed. A drop hammer test device is employed to conduct the dynamic impact experiments on various CGFB samples which have different dimensions and mix proportions and cured for different time. This test device can measure the acoustic energy loss generated in the process of impact. Therefore, the impact energy absorption power of the CGFB can be accurately measured.

2. It is found out that the higher the solid concentration of the CGFB is, the greater the energy absorption power of the CGFB is. Consequently, in practical prevention of rock bursts, it is more favorable to utilize the backfill materials with higher solids content to fill the mined-out voids.

3. The energy absorption power of the CGFB increases with the increase of its dimension. Thus in the prevention of rock bursts, it is better to fill the mined-out areas as full as possible.

4. In terms of the relationship between the impact energy absorption power of the CGFB and the impact energy, there is a critical value for the impact energy. When the impact energy is less than this value, the energy absorption power of the CGFB increases with increasing the impact energy. While if the impact energy is higher than the critical value, the increase of the impact energy leads to the decrease of the energy absorption power of the CGFB.

References

Bian Z, Dong J, Lei S, Leng H, Mu S, Wang H (2009) The impact of disposal and treatment of coal mining wastes on environment and farmland. Environ Geol 58(3):625–634

Cai MF, Wang JA, Wang SH (2001) Analysis of energy distribution and prediction of rockburst during deep mining excavation in Linglong Gold Mine. Chin J Rock Mech Eng 20(1):38–42 **(in Chinese)**

Cai YS, Zhao YZ, Wu SX, Sun HT (2013) Measurement of airborne sound insulation and the comparison between sound pressure and sound intensity method. J Vib Shock 32(21):65–68 **(in Chinese)**

Chugh YP, Deb D, Biswas D (2003) Underground placement of coal processing waste and coal combustion byproducts based paste backfill for enhanced mining economics. Mining in 21st Century, Proceedings of 19th World Mining Congress, New Delhi, pp. 1327–1341

Cui ZD, Sun HH (2010) The preparation and properties of coal gangue based sialite paste-like backfill material. J China Coal Society 35(6):896–899

Deng DQ, Gao YT, Wu SC, Yu WJ (2010) Experimental study of destructive energy dissipation properties of backfill under complicated stress condition. Rock Soil Mech 31(3):737–742 **(in Chinese)**

Dou LM, He XQ (2001) Theory and technology of rock burst prevention. China University of Mining and Technology Press, Xuzhou **(in Chinese)**

Dou LM, Zhao CG, Yang SG, Wu XR (2006) Prevention and control of rock burst in coal mine. China University of Mining and Technology Press, Xuzhou **(in Chinese)**

Du GH, Zhu ZM, Gong XF (2001) Acoustics foundation, 2nd edn. Press of Nanjing University, Nanjing **(in Chinese)**

Fall M, Samb SS (2009) Effect of high temperature on strength and microstructural properties of cemented paste backfill. Fire Safety J 44(4):642–651

Horiuchi S, Kawaguchi M, Yasuhara K (2000) Effective use of fly ash slurry as fill material. J Hazard Mater 76:301–337

Jiang YD, Pan YS, Jiang FX, Dou LM, Ju Y (2014) State of the art review on mechanism and prevention of coal bumps in China. J China Coal Soc 39(2):205–213 **(in Chinese)**

Karfakis MG, Bowman CH, Topuz E (1996) Characterization of coal-mine refuse as backfilling material. Geotech Geol Eng 14(2):129–150

Lin DN, Chen SR (2005) Experimental study on damage evolution of rock under cyclical impact loadings. Chin J Rock Mech Eng 24(22):4094–4098 **(in Chinese)**

Liu H, Liu Z (2010) Recycling utilization patterns of coal mining waste in China. Resour Conserv Recy 54:1331–1340

Liu ZX, Li XB, Zhao GY, Li QY, Wang WH (2010) Three-dimensional energy dissipation laws and reasonable matches between backfill and rock mass. Chin J Rock Mech Eng 29(2):344–348 **(in Chinese)**

Zhang QL, Wang XM (2007) Performance of cemented coal gangue backfill. J Cent South Univ Technol 14(2):216–219

Zheng BC, Zhou HQ, He RJ (2006) Experimental research on coal gangue paste filling material. J Mining Safety Eng 23(4):460–463